Superconductor Science and Technology

Effect of a DC transport current on the AC loss in no-insulation *Re*BCO racetrack coils exposed to AC parallel magnetic field at 77 K and 4.2 K

OPEN ACCESS
IOP Publishing
Superconductor Science and Technology
Supercond. Sci. Technol. **36** (2023) 075003 (10pp)
https://doi.org/10.1088/1361-6668/acd666

Effect of a DC transport current on the AC loss in no-insulation *Re*BCO racetrack coils exposed to AC parallel magnetic field at 77 K and 4.2 K

Jeroen ter Harmsel*, Simon Otten, Marc Dhallé and Herman ten Kate

Faculty of Science and Technology, University of Twente, Enschede, The Netherlands

E-mail: j.terharmsel@utwente.nl

Received 8 March 2023, revised 25 April 2023
Accepted for publication 17 May 2023
Published 25 May 2023

Abstract

*Re*BCO coils are developed as DC field coils in linear motor systems to increase the force density, in favor of permanent magnets. Such coils have to sustain a relatively large heat load stemming from the AC magnetic field environment in which they operate. The use of no or partial turn-to-turn insulation can make them more stable against the effects of local heating. Conversely, the radial electrical connections in no-insulation (NI) coils allow for large coupling currents, causing additional AC loss on top of the already significant heat load. Here we report on the AC loss in sub-scale NI, 4 mm wide single-tape, *Re*BCO racetrack coils exposed to parallel-to-the-tape magnetic field in the frequency range of 10^{-4} to 1 Hz at 77 K and 4.2 K, while carrying a DC transport current. AC loss is measured magnetically and electrically. The main goal of these experiments is to validate our 2D numerical model, which provides more insight into the origin of the AC loss. At low frequencies, inter-turn coupling currents are spread more or less homogeneously throughout the winding pack. Whereas at high frequencies, the skin effect causes shielding of the interior of the coil and large induced currents only occupy the coil's outer surface.

Keywords: AC loss, no-insulation coil, ReBCO, coupling loss

(Some figures may appear in colour only in the online journal)

1. Introduction

In recent years, high-temperature superconducting *Re*BCO tapes have been introduced in industrial applications, such as naval propulsion motors [1] and a wind turbine [2]. The main driver behind these developments is that *Re*BCO coils are able to produce higher magnetic fields than conventional permanent magnets. In actuators, this enables a higher force density, making them interesting for application in e.g. photolithography machines [3], where a reticle has to be accelerated in rapid repetition [4]. In this particular application, *Re*BCO stator coils experience a time-varying, non-sinusoidal magnetic field from the moving armature, which has an order-of-magnitude amplitude and frequency of 100 mT and 10 Hz, with higher-order harmonics. This produces a potentially high heat load in the form of AC loss in the superconducting stator coils, which increases further by the presence of a

* Author to whom any correspondence should be addressed.

DC transport current [5]. Photolithography machines need to operate reliably for many years with minimal downtime, so both the risk and the consequences of coil quenching must be minimized.

One possible way to mitigate the impact of local heating is to use no-insulation (NI) coils. It is well known that NI coils are less susceptible to local defects in *Re*BCO tapes and less likely to suffer irreparable damage in the case a quench does occur, because they allow current to bypass a local normal zone or hot spot through the turn-to-turn contact resistance R_{ct}, thus preventing a burn-out. A downside of using such coils in an AC magnetic field environment is the potential of additional loss, specifically coupling loss. In this paper, we therefore investigate the AC loss in sub-scale NI *Re*BCO racetrack coils to assess their applicability as stator coils in a high-dynamic superconducting linear motor (HSLM) system.

Ever since their conception [6], a lot of research has been invested in NI coils. Extensive efforts have for instance been made to control R_{ct} by co-winding various materials [7], by laminating the conductor surface [8] or by impregnating with solder [9].

Less has been published on AC loss in such coils. Kim *et al* [10] measured the AC loss due to an AC current in NI pancake coils with various co-wound tapes. They found the lowest AC loss in coils with the lowest R_{ct} value because part of the current bypasses the turns radially. AC loss reduction by this same mechanism is also observed by Zhang *et al* [11].

AC loss in insulated and NI coils exposed to external ripple fields is reported on by Wang *et al* [12]. They found that NI coils have much higher AC loss, stemming from induced currents generating Joule heating in the turn-to-turn resistance. Numerical calculations show that the skin effect causes most induced current to flow in the outer turns while shielding the interior.

Li *et al* [13] demonstrated the characteristics of coupling loss in partially coupled stacks of *Re*BCO tapes. Their 2D numerical model makes a distinction between loss occurring in the soldered contacts and in the superconductor itself. The latter tends to increase significantly at higher frequencies, which has been demonstrated experimentally as well.

The current distribution inside NI *Re*BCO pancake coils in a changing magnetic field applied parallel to the tapes' surface has been studied by Zhong *et al* [14]. They report on induced screening currents in the superconductor and remnant magnetic field, using a similar experimental set-up and winding pack homogenization method to this work.

Here we present experimental data on the AC loss in single 4 mm tape-based NI *Re*BCO racetrack coils carrying a DC transport current in an external AC magnetic field, applied parallel to the wide face of the tape. The experiments cover transport currents from 0 to 600 A and applied magnetic field frequencies from 0.5 mHz to 1.25 Hz. Measurements are performed both at 77 K and 4.2 K. The DC current/AC field scenario is representative of what the DC stator coils in linear motors experience, except for the frequency, which can be much higher in real motor applications. This work expands on the results published earlier in [15, 16]. We use a 2D numerical model to explain the findings and demonstrate that this computation method can be used very well as a design tool to compute AC loss in motor drives using *Re*BCO coils.

Section 2 introduces the different loss mechanisms that contribute in the experiment by evaluating the numerical model in three distinct frequency domains. The effect of a DC transport current on the AC loss is also discussed. Section 3 describes the dedicated sample coils that were made for this experiment as well as the experimental set-up and instrumentation. Section 4 presents the results of the AC loss experiments, considering both magnetization- and transport current losses as a function of applied field frequency and compares them to the model predictions.

2. Theory

2.1. AC loss components

Consider a racetrack coil placed in an external time-varying magnetic field along the z-axis, as shown schematically in figure 1.

A current will be induced that tends to counteract the flux change produced by the external field, this current is referred to here as the 'magnetization current'. The loss component generated by this current is called 'magnetization loss' Q_{mag}. When the applied magnetic field is uniform, the magnetization current will flow along the winding direction of the coil, mostly following the superconducting path and only crossing in-between turns to close the current loop. The ohmic dissipation caused by the crossing-over of the magnetization current is called the 'coupling loss' $Q_{coupling}$. When the magnetization current approaches the critical current density of the tape J_c, loss is also generated in the superconductor according to the usual $E(J)$ relation, referred to as the 'superconductor loss' $Q_{superconductor}$. The induced magnetization current density J_{mag} can reach this level at high frequencies, where the skin effect concentrates current in a shell at the outer surface. The magnitude of J_{mag} decays inward over a characteristic length scale, the skin depth $\delta = \sqrt{\rho_\perp \sin^2(\alpha)/\pi\mu_0 f}$ [15]. Here, $\rho_\perp$ is the effective transverse resistivity of the coil, f is the frequency of the applied magnetic field and $\alpha = d_{turn}/\ell_{turn}$ is the winding angle, i.e. the angle between the path of the conductor and the axis of the straight leg of the racetrack. The sum of the coupling loss and superconductor loss forms the magnetization loss.

$$Q_{mag} = Q_{coupling} + Q_{superconductor}\,. \tag{1}$$

Running a DC transport current I_{dc} through the superconducting coil while it is exposed to the AC magnetic field can create additional 'transport current loss' Q_{trans}. The magnetization current displaces the transport current inside the superconductor, requiring the power supply to do extra work to maintain I_{dc} at a constant level [5]. Q_{trans} is further enhanced when part of I_{dc} flows through a resistive medium. This occurs when

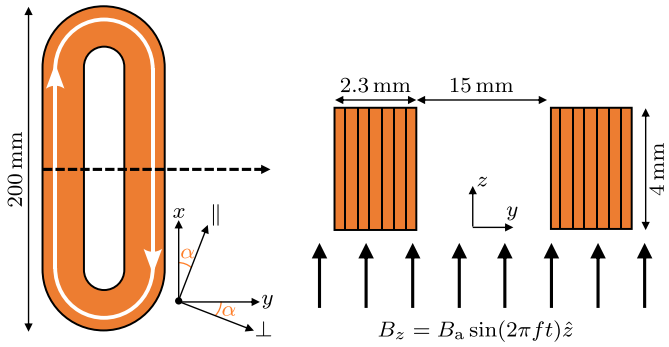

Figure 1. Schematic representation (not to scale) of the sample coil in applied magnetic field B_z parallel to the wide tape surface, showing a top view (left) and a cross-section of the straight legs (right). The white arrow indicates the path of the magnetization current that is induced by B_z. The superconducting tape lies at a small angle α with respect to the x-axis to account for turn thickness.

the current starts to bypass turns as it approaches the critical current I_c (which is typical for NI coils) and when magnetization currents occupy the full width of the superconducting tape. The total AC loss Q_{tot} in this system is then given by:

$$Q_{tot} = Q_{mag} + Q_{trans}\,. \tag{2}$$

2.2. Numerical model

We have developed a 2D numerical model to predict AC loss generated in *Re*BCO racetrack coils. A detailed description of this computational method can be found in [15]. In brief, it calculates the current distribution in a 2D cross-section of a *Re*BCO racetrack coil by solving an integral form of Maxwell's equations [17, 18]. The winding pack with all its components is approximated as a homogeneous material with anisotropic resistivity, with the effective transverse resistivity $\rho_\perp$ perpendicular to the turns and the power law $\rho \propto (J/J_c)^{n-1}$ along the path of the conductor. In the model result of figures 2 and 3, we assume a uniform J_c, thus neglecting the I_c-variance between turns because the main focus of these results is to demonstrate the effect of the coil's time constant on the loss characteristics. A $J_c(B)$-characteristic can be included in the model, but this is only done for the measurement data at 4.2 K, since we measured the magnetic field dependency of the tape only at this temperature. A similar homogenization method is used in [19]. In the remainder of this section, we briefly review the various loss components predicted by the model.

The character of the AC loss depends strongly on the ratio of the frequency of the applied magnetic field f and the characteristic frequency f_c of the sample coil, with $f_c = 1/2\pi\tau = R_c/2\pi L$. Here L is the usual self-inductance and R_c the characteristic resistance often used to describe charge- or discharge experiments [20].

Consider an NI *Re*BCO racetrack coil in a sinusoidal, homogeneous magnetic field of amplitude B_a along the z-axis. The racetrack coil carries a DC current and produces a DC magnetic field in the positive z-direction. Magnetization currents oppose the flux change due to the external AC magnetic field, so when $dB/dt < 0$ they run parallel to I_{dc} and increase the parallel net current density $J_\parallel$. As an example, consider a coil with a characteristic frequency of 2.4 mHz, effective transverse resistivity of 0.82 μΩm and a homogeneous and constant I_c value of 72 A and an n-value of 30. One tape is 4 mm wide and 125 μm thick, so the effective J_c of the homogenized winding pack becomes 144 A mm^{-2}. The coil dimensions are set equal to that of the sample coils discussed in section 3 (see figure 1).

We define three distinct frequency ranges where different loss mechanics contribute: $f \ll f_c$, $f \gtrsim f_c$ and $f \gg f_c$. In the model, the total AC loss density in W/m^3 is calculated as $p_{tot} = E \cdot J$, which we separate into $p_\parallel = E_\parallel J_\parallel$ and $p_\perp = E_\perp J_\perp$, the losses caused by currents flowing parallel and perpendicular to the superconductor, respectively. This distinction will shed light on how AC loss is generated in our coils. Figures 2 and 3 show the evolution of these losses during one magnetic field cycle, with the phase $\theta = 2\pi$ corresponding to one full period of the AC magnetic field. The three distinct frequency regimes are shown separately, each time for two DC current levels (0% and 70% of I_c, respectively). Since they are qualitatively different, we describe each frequency regime separately. Corresponding typical current distributions are plotted in figure 4.

2.2.1. $f \ll f_c$ (0.1 mHz). Here, induced currents can decay faster than the magnetic field oscillates, so they distribute homogeneously throughout the winding pack. As a result, the whole coil experiences the same applied magnetic field and AC loss is spread out evenly over the winding pack. When $I_{dc} = 0$ A (figure 2(b)), the only power dissipated is due to the coupling currents flowing perpendicular to the superconductor. $P_\parallel$ is negligible, because magnetization currents lie far below I_c. Adding a transport current (figure 3(b)) produces a flux flow resistance according to the usual $E(J)$ power law because of the finite n-value and thus a DC component is added to $P_\parallel$. The contribution of dynamic resistance, see also the measured and modeled Q_{trans} data in figure 8, is still relatively small here but becomes larger and detectable at around f_c. Furthermore, rather than the familiar instantaneous loss variation with $2f$, characteristic of 'straightforward' ohmic losses, $P_\parallel$ oscillates with the same frequency f as the external AC field. Indeed, I_{dc} breaks the symmetry causing the net current density $J_\parallel$ to be larger at $\theta = \pi$, when the transport- and magnetisation currents flow in the same direction, than at $\theta = 2\pi$, when they oppose each other. In this low-frequency limit, $J_\parallel$ is homogeneous throughout the winding pack, see figure 4.

2.2.2. $f \gtrsim f_c$ (10 mHz). In this regime, the skin depth δ is smaller than the coil dimensions. Currents induced by the applied magnetic field are therefore largest at the outer surface of the coil and decay inward, see figure 4. As a result, the inner part of the coil becomes partially shielded from the magnetic

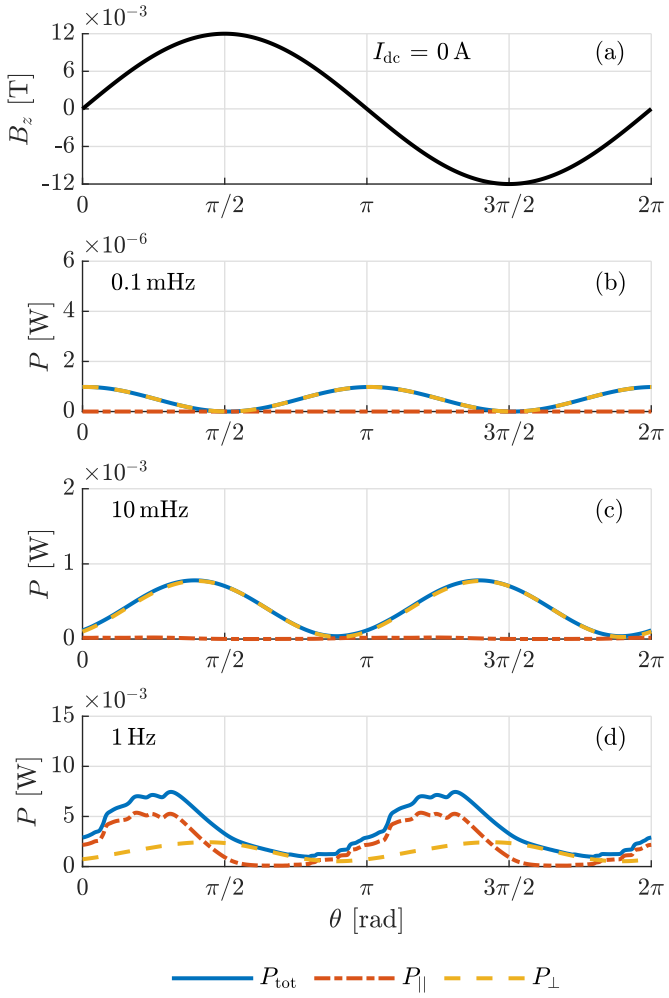

Figure 2. Modeled AC loss during a single magnetic field cycle, separated into losses caused by currents running parallel and perpendicular to the superconductor. The uniform applied magnetic field is shown in (a). The loss due to parallel and perpendicular currents, as well as the sum of the two, are shown in (b)–(d) for field frequencies of 0.1 mHz, 10 mHz and 1 Hz, respectively. $I_c = 72$ A and $I_{dc} = 0$ A.

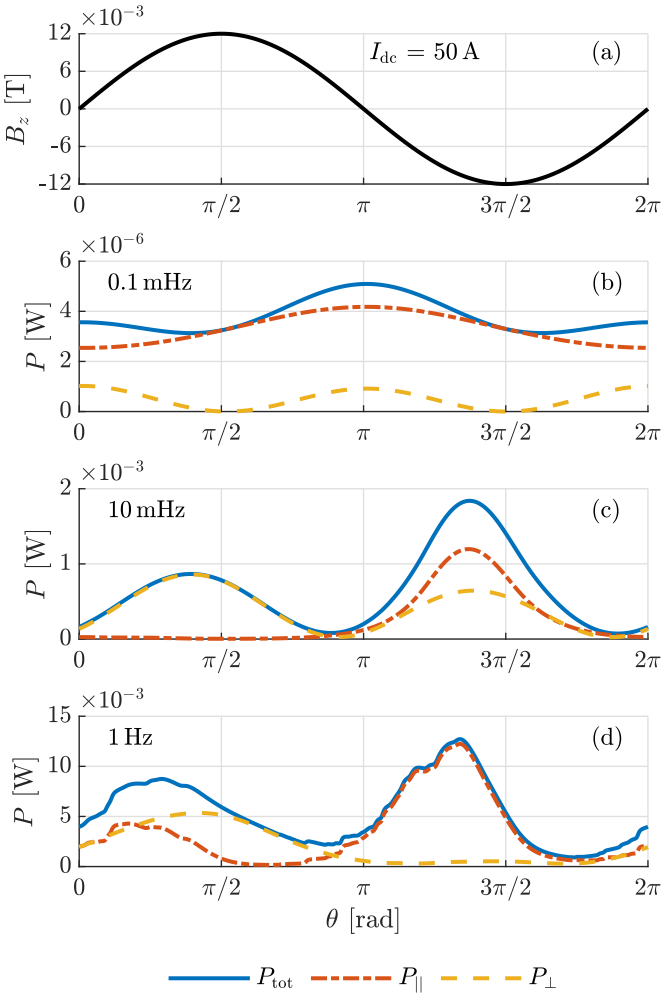

Figure 3. Modeled AC loss during a single magnetic field cycle, separated into losses caused by currents running parallel and perpendicular to the superconductor. The separate plots are like in figure 2, but this time with a DC current of 50 A injected in the coil.

field. Because of this shielding effect, dissipation is concentrated at the outer surface of the coil. The loss is somewhat phase-shifted with respect to B_z. However, like in the low-f regime, the bulk of the dissipation is still caused by coupling currents, see figure 2(c). Adding a transport current causes a large peak in $P_{||}$ just before $\theta = 3\pi/2$ (figure 3(c)). Here, magnetization currents align with I_{dc} and push the net current in the superconductor close to I_c. When the magnetization current polarity is opposite (around $\theta = \pi/2$), minimal change in AC loss with respect to the 0 A result is observed because $J_{||}$ is reduced and thus does not contribute significantly to $P_{||}$ at this point in the field cycle.

2.2.3. $f \gg f_c$ (1 Hz). At sufficiently high frequencies the skin depth δ becomes so small that the magnetization current density approaches J_c in the skin even in the absence of a transport current. This causes a strong increase in $P_{||}$ at the outer surface by fully magnetizing the superconductor (figure 2(d)).

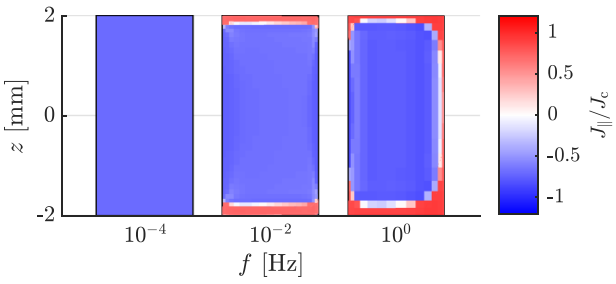

Figure 4. Computed current density (normalized with J_c) flowing parallel to the superconductor in the NI winding pack that is subjected to a 12 mT parallel magnetic field of selected frequencies. The coil carries a transport current of $I_{dc}/I_c = 0.7$, indicated in blue in this figure. Only the right leg of the racetrack coil from figure 1 is shown. The current density in this figure is a snapshot when the applied field is 12 mT, i.e. $\theta = \pi/2$. The magnetization current is such that an opposing field (in the negative z-direction) is produced. At $f = 1$ Hz, the magnetization currents are concentrated at the outer surface, completely reversing the current in the outer nodes.

The inside of the coil is nearly entirely shielded from the external magnetic field, so dissipation is heavily concentrated at the outer surface. The shielding distorts the magnetic field

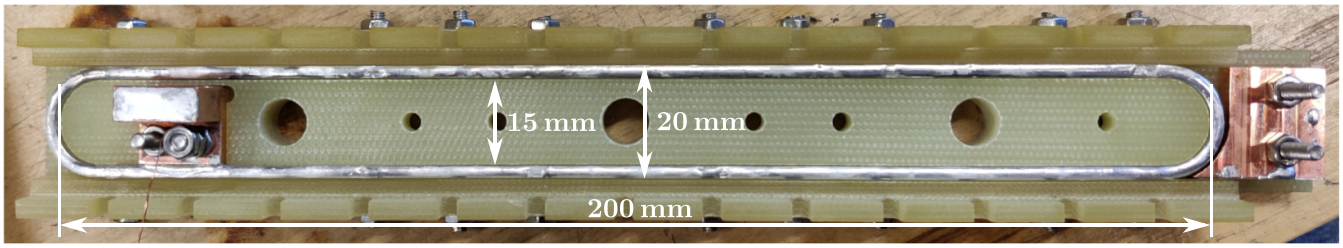

Figure 5. One of the two NI *Re*BCO racetrack coils used in the AC loss experiment. InSn solder connects the turns to each other. Copper current terminals are soldered to the inner and outer turn. The coil is encased on all sides by a GFRP structure (top cover removed in this photograph). Additional coil dimensions are given in figure 1.

and a relatively large field is observed at the outer surface. Adding a transport current increases $P_{\parallel}$ in the second half of the magnetic field cycle (figure 3(d)), similar to what happens at 10 mHz. A second interesting effect is observed around $\theta = \pi/2$, where the magnetization current opposes I_{dc} and forces it to flow perpendicular to the turns. This results in a large peak in $P_{\perp}$ around $\theta = \pi/2$. Figure 4 also clearly shows this: a current opposing I_{dc} runs along the outer surface of the coil.

To validate this model, an experimental campaign was set up on small NI *Re*BCO racetrack coils exposed to a uniform AC magnetic field. By covering a wide frequency range, all the loss predictions discussed in this section are verified. In the next section, the experimental set-up, the measurement procedure and the fabricated sample coils are presented.

3. Experimental set-up

3.1. No-insulation racetrack coil

Two identical 18-turn NI *Re*BCO racetrack coils are fabricated with single 4 mm wide, InSn solder-coated, tape from SuperOx with a self-field I_c of 123 A at 77 K (figure 5). In the set-up, two NI racetrack coils are connected in anti-series to minimize the net torque on the background magnet. For details on the experimental set-up, see [16]. After winding, the turns are electrically connected by heating the whole coil to 150 °C on a hot plate, while adding additional InSn solder from above. This essentially shorts the turns and allows the transport of current from one turn to the next with minimal dissipation. The coil shape is maintained by clamping the winding pack from both sides. Such a solder-filled coil was first introduced by Li *et al* [9]. The racetracks are characterized for critical current, generated magnetic field and time constant. The full results are reported in [15] and summarized in table 1. A single coil time constant τ is determined by fitting an exponential decay to a sudden discharge test. This models the coil as a straightforward LR-circuit, although some variance in the decay rate is observed during discharging. We incorporate this as an uncertainty in the τ-value. The ∼25% difference in R_{ct} value between the two coils is likely due to slight variations in the soldering procedure. The self-inductance L of both coils is calculated to be 72 μH.

Table 1. Measured characteristics of the two racetrack coils. The time constant τ is determined with a sudden discharge test and the contact resistance R_{ct} is calculated from it. The coil I_c is determined measuring the voltage over the coil, assuming an electric field criterion of 100 μVm^{-1}. Note that this critical current value is about 20% higher than the one used in the numerical model discussed in section 2 due to current bypassing through the soldered turns leading to a more gradual transition. The n-value could not be accurately determined for this same reason. For the model we assume a tape n-value of 30.

Coil #	T (K)	τ (s)	R_{ct} ($\mu\Omega cm^2$)	Coil I_c (A)
1	77	58 ± 1	1.14 ± 0.02	85
1	4.2	117 ± 2	0.56 ± 0.01	>700
2	77	74 ± 1	0.89 ± 0.01	93
2	4.2	155 ± 4	0.42 ± 0.02	>700

Table 2. Parameter space of the two AC loss experiments in liquid nitrogen and liquid helium.

T (K)	77	4.2
Field orientation	parallel	parallel
B_a (mT)	12	100
I_{dc} (A)	0–60	0–600
f (mHz)	0.5–1250	0.5–200
B_{dc} (mT)	0	500

3.2. Experimental conditions

The AC loss measurements are performed with a uniform, sinusoidally time-varying magnetic field applied in the z-direction, i.e. parallel to the wide face of the superconducting tape. This geometry is schematically shown in figure 1. A first set of measurements is performed in liquid nitrogen at 77 K, followed by a second set in liquid helium at 4.2 K. The explored parameter space is given in table 2. Going to lower temperatures enables a higher applied field amplitude from a NbTi dipole magnet and a larger transport current in the racetrack coils. However, measurements at 4.2 K span a more narrow frequency range, due to voltage limitations of the power supply. At 4.2 K, the used InSn solder in-between the turns is superconducting [21]. To prevent this from interfering with the measurement, a DC offset field B_{dc} of 0.5 T is superimposed on the AC magnetic field, driving the solder in the normal state.

3.3. Measurement systems

The AC loss measurements are performed in a set-up capable of measuring magnetization loss Q_{mag} with pick-up coils as well as transport current loss Q_{trans} with voltage taps. Further details on this set-up can be found in [16]. Q_{mag} is calculated by integrating the product of the z-component of the magnetization of the racetrack coils m_z and the applied magnetic field B_z over a complete field cycle:

$$Q_{\mathrm{mag}} = -\oint B_z \cdot \mathrm{d}m_z = \int_0^{2\pi/\omega} B_z \cdot \dot{m}_z \,\mathrm{d}t\,. \tag{3}$$

The relation between the net voltage over the pick-up circuit V_{pu} and m_z is derived analytically from the relative positions of the racetrack and pick-up coils:

$$V_{\mathrm{pu}} = -\frac{\mu_0}{2\pi} K \dot{m}_z\,, \tag{4}$$

where the geometrical factor K is:

$$K = \sum_i \frac{1}{2y_s} \ln\left(\frac{\sqrt{(y_i - y_s)^2 + (z_i - z_s)^2}}{\sqrt{(y_i + y_s)^2 + (z_i - z_s)^2}}\right). \tag{5}$$

This expression is a sum over all pick-up coil wires at positions (y_i, z_i) for a leg of the racetrack coil at (y_s, z_s). The derivation of equation (5) is described in [15].

The net voltage over the pick-up circuit V_{pu}, from which Q_{mag} is calculated, is measured with two devices. At frequencies of 20 mHz and above, it is recorded with a lock-in amplifier. Using as reference the voltage driving the power supply of the AC dipole magnet. The phase delay between this function generator signal and B_z is corrected for with a second lock-in amplifier, which records the dipole current with respect to the same reference signal. This phase delay can be significant, approximately 10° at 1 Hz, and must therefore be taken into account when calculating the AC loss from V_{pu}. The settling time of several field cycles required by the lock-in amplifier makes it impractical for frequencies below ∼20 mHz. Therefore, V_{pu}, as well as B_z, are recorded with a nanovolt meter at these frequencies.

A pair of voltage taps on the current terminals of a single coil is used to measure V_{coil}. The voltage is recorded by a Keithley 2000 multimeter. Only a single coil is probed in order to limit the background offset stemming from the joint resistance, since the voltage pair also includes the resistance of the copper terminals and the solder joint between the coil and the terminals. The stationary transport current I_{dc} is measured with a zero-flux transducer. Q_{trans} is then calculated as:

$$Q_{\mathrm{trans}} = I_{\mathrm{dc}} \int_0^{2\pi/\omega} V_{\mathrm{coil}}(t)\mathrm{d}t\,. \tag{6}$$

Integrating over a full field cycle removes any inductive component. Due to the joint resistances, an offset loss value is measured at zero magnetic field, which is subtracted from subsequent measurements.

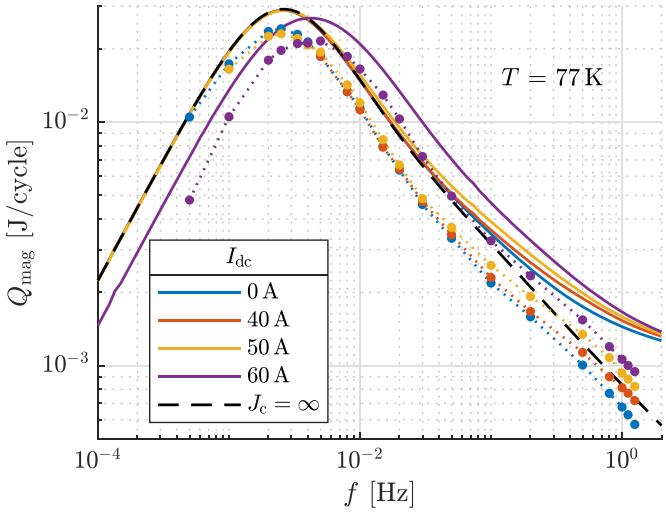

Figure 6. Frequency dependence of the magnetization loss in the NI *Re*BCO racetrack coils at 77 K, in a 12 mT amplitude magnetic field applied parallel to the tapes' surface, plotted for different stationary transport currents. The measured data are the colored discrete symbols connected by dotted lines. The lines show the numerical results for comparison with either $I_c = 72$ A (solid, colored) or $J_c = \infty$ (dashed, black).

4. Results and analysis

4.1. Magnetization loss

Figures 6 and 7 show the magnetization loss in J/cycle as a function of frequency f for several DC transport currents at 77 K and 4.2 K, respectively. In both figures, the AC loss data generally follow the model predictions quite satisfactorily. When $f \ll f_c$, Q_{mag} scales with f, which indicates that the coupling currents occupy the full volume of the winding pack as predicted in section 2. When $f \gg f_c$, Q_{mag} scales with $1/\sqrt{f}$ because of the skin effect. The transition between the two regimes, indicated by a peak in Q_{mag}, occurs at the characteristic frequency $f_c = 1/2\pi\tau$ (2.5 mHz at 77 K and 1.2 mHz at 4.2 K). Note that the corresponding τ-values (64 s and 133 s, respectively) correspond well to the average of the values found in the independent discharge experiments, see table 1.

Adding a DC transport current to the racetrack coil exposed to the AC parallel magnetic field increases the AC loss when $f \gg f_c$, as can be seen in both figures 6 and 7. The magnitude of the increase in AC loss scales with I_{dc} and starts at lower f for larger I_{dc}, since the superconductor is saturated at a progressively larger skin depth. A more detailed explanation of the acting loss mechanisms is given in section 2.

The 60 A data in figure 6 are noticeably shifted to higher frequencies, indicating a decrease in τ. This is likely caused by the presence of flux flow resistance R_{sc} in the superconductor when the transport current is close to I_c. This elevated resistance results in a smaller time constant: $\tau = L/(R_c + R_{\mathrm{sc}})$.

Measured data are compared to numerical simulation results, presented as solid lines in figures 6 and 7. A constant I_c value of 72 A at 77 K is assumed, but an experimentally

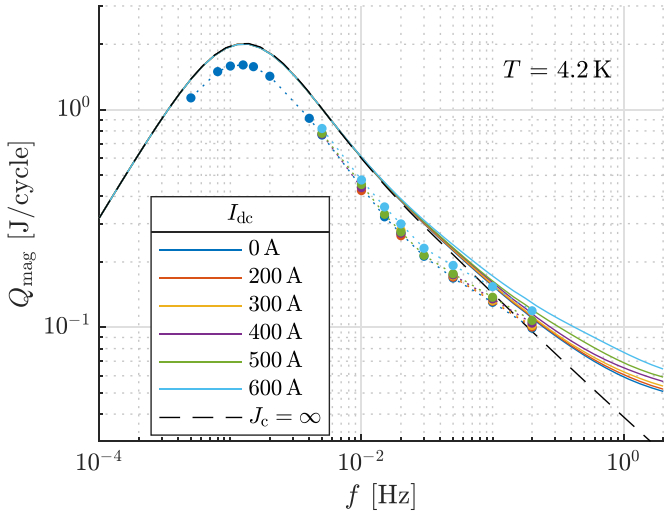

Figure 7. Frequency dependence of the magnetization loss in the NI *Re*BCO racetrack coils at 4.2 K, in a 100 mT amplitude magnetic field applied parallel to the tapes' surface, plotted for different stationary transport currents. The measured data are the colored discrete symbols connected by dotted lines. The lines show the numerical results for comparison with the independently measured $J_{\mathrm{c}}(B)$ (solid, colored) and with $J_{\mathrm{c}} = \infty$ (dashed, black).

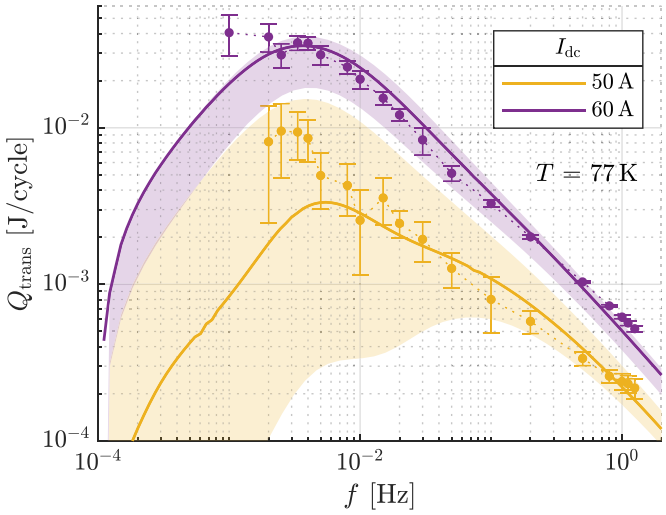

Figure 8. Frequency dependence of the transport current loss in one NI racetrack coil at 77 K, in a 12 mT amplitude magnetic field applied parallel to the tapes' surface, plotted for two stationary transport current levels of 50 and 60 A. The measured data are the colored discrete symbols connected by dotted lines. The solid lines and shaded areas show the numerical results and uncertainty bands, respectively. This model uncertainty is derived by calculating the minimum and maximum AC loss at each frequency over a range of coil properties ($I_{\mathrm{c}} = 72 \pm 4$ A, $n = 30 \pm 5$) to account for non-uniformity in the winding pack.

determined $J_{\mathrm{c}}(B)$ relation is used at 4.2 K. An n-value of 30 is assumed for both. An additional model solution for $I_{\mathrm{c}} = \infty$ is shown as a dashed line to demonstrate the effect the critical current value has on the AC loss. The effective transverse resistivities $\rho_{\perp}$ of the modeled coils are 0.82 μΩm and 0.40 μΩm at 77 K and 4.2 K, respectively. These values are determined from the average time constant observed in the discharge experiments, see also table 1. A qualitative agreement between experimental and numerical data is observed: Q_{mag} increases at low f, reaching a peak around f_{c} and decreasing at higher f. The effect of transport current on Q_{mag} is also reproduced well by the model. It increases the AC loss at high frequencies, more so and starting from lower f, if I_{dc} is larger. The change in time constant observed in figure 6 is also reproduced, which means that the approximation of constant I_{c} is reasonable. In both figures, the measured magnetization loss consistently lies approximately 20% below the calculated values. This systematic difference is likely caused by uncertainties in the positioning of the pick-up coils and the corresponding calibration factor (equation (5)).

Model and experiment deviate substantially for $f \gtrsim 0.1$ Hz at 77 K. The model predicts the loss to saturate at a constant value, caused by hysteresis losses in the fully penetrated superconductor. In this range, the experiment does not confirm the prediction. Instead, Q_{mag} continues to scale with $1/\sqrt{f}$. Since the data behave as was predicted for a coil with infinite J_{c}, it was initially thought that the current might bypass the superconductor to flow through the copper stabilizer instead. However, including such a parallel copper path to the superconductor also in the model did not have a noticeable effect on the AC loss. Interestingly, the onset of a plateau *is* observed experimentally at 4.2 K and at $f = 0.2$ Hz, across all the levels of transport current, see figure 7. Why this effect occurs at 4.2 K and not at 77 K is unclear at this moment and subject to further investigation. Frequencies higher than 0.2 Hz could not be studied for this field amplitude, because of limitations of the experimental set-up.

4.2. Transport current loss

Q_{trans} is supplied by the current source keeping I_{dc} constant under the effect of the alternating magnetic field. This is observed as a net DC offset voltage over the coils, as shown in figure 8. Only data at 77 K are presented here because the background offset voltage due to the joints was too large at 4.2 K. Q_{trans} starts to become significant at a given frequency where the sum of I_{dc} and the magnetization current approaches I_{c}, soon after which it reaches a maximum. Further increasing f causes the loss per cycle to decrease, due to increased shielding of the interior of the winding pack.

The experimental data in figure 8 are measured only in coil 1 to limit the background offset loss from the joints. They are compared to numerical model results obtained for a single coil with input parameters $I_{\mathrm{c}} = 72 \pm 4$ A, $n = 30 \pm 5$ and $\tau = 58$ s. The shaded area around the modeled curves show the sensitivity of the model to this variation in superconducting properties, which is particularly large at the lower end of the considered frequency range, before the peak in Q_{trans}. The modeled 50 A data are more susceptible to these variations because the influence of the uncertainty in the n-value becomes more pronounced as one moves further away from I_{c}.

At low frequencies and when $I_{\mathrm{dc}} \ll I_{\mathrm{c}}$, also the measured Q_{trans} data suffer from a relatively large uncertainty due to the importance of the DC background voltage compared to

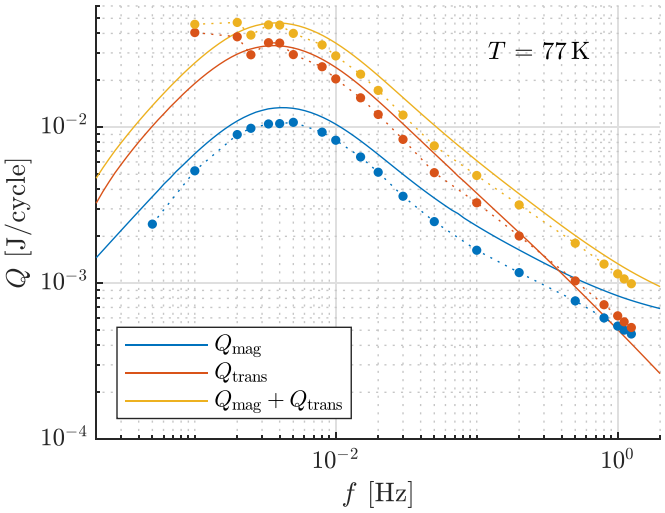

Figure 9. Frequency dependence of the measured transport and magnetization loss in a single NI racetrack coil at 77 K in a 12 mT amplitude AC magnetic field applied parallel to the tapes' surface, with a DC transport current level of 60 A. The discrete symbols connected by dotted lines are measured data and the solid lines are the numerical results. Data (measured and modeled) are separated into magnetization and transport current loss. The total loss is the sum of these components.

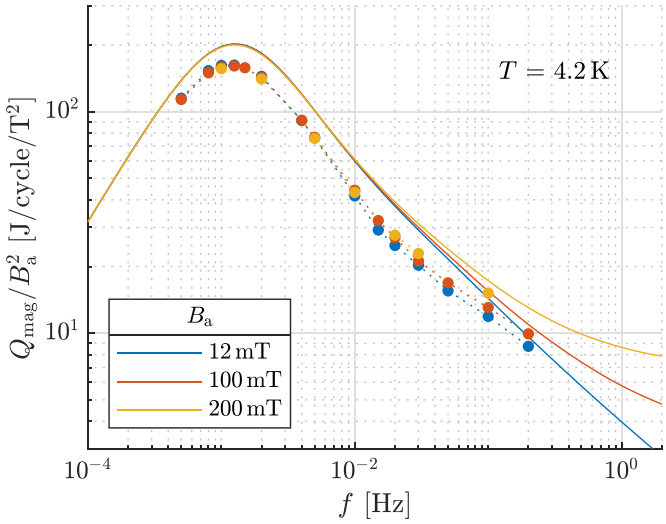

Figure 10. Frequency dependence of the magnetization loss in the NI *Re*BCO racetrack coils as a function of frequency at 4.2 K, in a magnetic field applied parallel to the tapes' surface and without a transport current. Data are plotted for different magnetic field amplitudes B_{a} and are normalized to B_{a}^2. The discrete symbols connected by dotted lines are measured data and the solid lines are model predictions.

the low AC loss, which makes it difficult to determine Q_{trans} accurately. Only when I_{dc} is close to I_{c} does the uncertainty on Q_{trans} become insignificant. Around $f = 1$ Hz, we systematically measure high Q_{trans} values than the model predicts. This may be explained by the model assumption of a constant J_{c} value, rather than a $J_{\mathrm{c}}(B)$ relation. The magnetic field dependence of J_{c} was not measured for this conductor at 77 K.

4.3. Loss components

Figure 9 compares the relative contributions of the different loss mechanisms in a single coil when testing at 77 K with a transport current of 60 A. Following equation (2), the total AC loss Q_{tot} is given by the sum of Q_{mag} and Q_{trans}. In the experiment, Q_{mag} and Q_{trans} are measured separately. In principle, Q_{tot} may be measured calorimetrically [16], but in this case the loss is too small to detect with our calorimeter at 77 K. Instead, simply the sum of Q_{mag} and Q_{trans} is plotted.

At different f, different loss mechanisms dominate. Given that the coil is DC-excited at roughly 80% of I_{c}, Q_{trans} is much larger than Q_{mag} for $f < f_{\mathrm{c}}$. For smaller I_{dc} values, Q_{trans} is typically small compared to Q_{mag}. Assuming that the transport current is homogeneously displaced by the magnetization currents, the total current stays well below I_{c} everywhere. When $f > f_{\mathrm{c}}$, the induced current is more concentrated near the outer surface of the coil and the loss per cycle decreases. Note that Q_{mag} decreases less steeply than Q_{trans}. This can be qualitatively understood as due to the induced currents that shield most of the interior of the winding pack, allowing I_{dc} to flow undisturbed throughout most of the coil.

4.4. Effect of magnetic field amplitude

The measurements at 4.2 K are performed at three magnetic field amplitudes: 12, 100 and 200 mT. Coupling loss is known to vary as B_{a}^2 [22], so to compare the data, they are normalized by this factor. The normalized AC loss is plotted in figure 10, along with the corresponding model predictions.

For frequencies up to ∼10 mHz the data measured at the three amplitudes virtually coincide, i.e. the B_{a}^2 scaling holds. Because the coil behaves linearly when $E_{\parallel} \approx 0$, i.e. when $J_{\parallel} < J_{\mathrm{c}}$, the time constant remains the same and the three lines all show a peak at the same value of f_{c}. When $J_{\parallel}$ approaches J_{c}, a shift in f_{c} is observed, such as in figure 6. However, deviations become apparent at the higher frequencies. This behavior is also predicted by the model. The deviations are caused by magnetization currents approaching the critical current I_{c}. This occurs at a lower frequency when the applied field is larger since the induced current is larger. Unfortunately, the set-up did not allow to probe even higher magnetic fields or frequencies.

5. Conclusion

Turn-to-turn coupling loss in no-insulation single-tape *Re*BCO racetrack coils has been studied both numerically and experimentally in a uniform, time-varying magnetic field, over a range of magnetic field frequencies on either side of the coils' characteristic frequency, at 77 K and 4.2 K, and in combination with a stationary transport current up to close to the critical current. Two dedicated solder-filled coils were fabricated

to achieve sufficiently long time constants in the order of minutes.

It is observed that the coil's time constant and associated characteristic frequency f_c, determine the main characteristics of the coupling loss in these NI coils. Applying an alternating magnetic field with a frequency below f_c induces coupling currents throughout the winding pack and the loss, expressed in J/cycle scales linearly with frequency. Above f_c, due to the skin effect, induced currents can no longer penetrate the full depth of the winding pack, but rather flow along the outer edge.

Combining these magnetization currents with a DC transport current increases the AC loss especially for frequencies above f_c. As the skin depth is reduced, the induced magnetization current density increases. At a given point the sum of the shielding and DC transport currents approaches the critical current I_c, increasing the resistance in the current path and thereby increasing the loss. Higher transport currents cause this effect to occur at lower frequencies and to become more pronounced. Under these conditions also the transport current loss becomes noticeable. It arises at a frequency where the combined magnetization current and transport current exceed the critical current locally and is usually small relative to the magnetization loss, unless the transport current is close to the critical current I_c, approximately at 80%.

The experimental results confirm the predictions of our 2D numerical model. Model and experiments typically agree within 20%, which is quite good considering the data are not fitted to the model after measuring. Instead, the model predicts the losses a priori, using as input the coil geometry and its independently measured I_c value, n-factor and decay time constant. The model consistently overestimates the magnetization loss somewhat, which is likely due to the uncertainty in the placement of the pick-up coils. The transport current loss is also reproduced reasonably well by the model. However, it is predicted that the AC loss will reach a plateau at $f \gg f_c$, but this was not observed experimentally. We can use the numerical model to gain insight into current and loss distributions inside such coils when they are used in an AC magnetic field environment. It can also be used as a design tool for linear superconducting motor drives to determine optimal coil parameters, such as geometry and operating current.

Data availability statement

The data that support the findings of this study are available upon reasonable request from the authors.

Acknowledgments

This publication is part of the project High-dynamic Superconducting Linear Motor (with Project Number 15362) of the research programme High Tech Systems and Materials which is financed by the Dutch Research Council (NWO) and supported by participating industrial partners: ASML, VDL-ETG and Prodrive Technologies.

ORCID iDs

Jeroen ter Harmsel https://orcid.org/0000-0001-5512-0673
Simon Otten https://orcid.org/0000-0002-1369-6903
Marc Dhallé https://orcid.org/0000-0002-3883-3556
Herman ten Kate https://orcid.org/0000-0001-5597-3190

References

[1] Moon H, Kim Y-C, Park H-J, Yu I-K and Park M 2016 An introduction to the design and fabrication progress of a megawatt class 2G HTS motor for the ship propulsion application *Supercond. Sci. Technol.* **29** 034009
[2] Bergen A et al 2019 Design and in-field testing of the world's first ReBCO rotor for a 3.6 MW wind generator *Supercond. Sci. Technol.* **32** 125006
[3] De Bruyn B J, Jansen J W and Lomonova E A 2016 Comparison of force density of various superconducting linear motor types considering numerically evaluated AC losses *IEEE Trans. Appl. Supercond.* **26** 1–5
[4] Butler H 2011 Position control in lithographic equipment [applications of control] *IEEE Control Syst. Mag.* **31** 28–47
[5] Wilson M N 1983 *Superconducting Magnets* (Oxford: Clarendon)
[6] Hahn S, Park D K, Bascuñán J and Iwasa Y 2010 HTS pancake coils without turn-to-turn insulation *IEEE Trans. Appl. Supercond.* **21** 1592–5
[7] Lee T S, Hwang Y J, Lee J, Lee W S, Kim J, Song S H, Ahn M C and Ko T K 2014 The effects of co-wound Kapton, stainless steel and copper, in comparison with no insulation, on the time constant and stability of GdBCO pancake coils *Supercond. Sci. Technol.* **27** 065018
[8] Choi Y H, Kwon O J, Kim Y-G, Song J-B, Kim J H, Kim H-M and Lee H 2013 Thermal quench behaviors of no-insulation coils wound using GdBCO coated conductor tapes with various lamination materials *IEEE Trans. Appl. Supercond.* **24** 1–5
[9] Li Y, Hu D, Zhang J, Wu W, Li Z, Ryu K, Hong Z and Jin Z 2017 Feasibility study of the impregnation of a no-insulation HTS coil using solder *IEEE Trans. Appl. Supercond.* **28** 1–5
[10] Kim J, Nam S, Jeon H, Kim J, Jang J Y and Ko T K 2016 Experimental analysis on AC loss and fault current test of HTS coils co-wound with various inserted materials *IEEE Trans. Appl. Supercond.* **26** 1–5
[11] Zhang Z, Kim C H, Kim J G, Kvitkovic J, Pamidi S, Zhang M, Li J and Yuan W 2017 An experimental investigation of the transient response of HTS non-insulation coil *J. Supercond. Nov. Magn.* **30** 387–93
[12] Wang Y, Zhang M, Šouc J, Gömöry F, Weng F, Li J, and Yuan W 2020 AC losses of no-insulation high temperature superconductor (RE) Ba2Cu3Ox coils induced by ripple magnetic fields in machines
[13] Li S, Kováč J and Pardo E 2020 Coupling loss at the end connections of REBCO stacks: 2D modelling and measurement *Supercond. Sci. Technol.* **33** 075014
[14] Zhong Z, Wu W, Hong Z and Jin Z 2022 Experiment and numerical modeling of current distributions inside REBCO tapes of no-insulation superconducting magnet coils under time-varying fields *J. Supercond. Nov. Magn.* **35** 3177–88
[15] Otten S, ter Harmsel J, Dhallé M and ten Kate H H 2023 Calculation and measurement of coupling loss in a no-insulation ReBCO racetrack coil exposed to AC magnetic field *Supercond. Sci. Technol.* **36** 044002

[16] ter Harmsel J, Otten S, Dhallé M and ten Kate H 2022 Magnetization loss and transport current loss in ReBCO racetrack coils carrying stationary current in time-varying magnetic field at 4.2 K *Supercond. Sci. Technol.* **36** 015011
[17] Brandt E H 1994 Thin superconductors in a perpendicular magnetic ac field: general formulation and strip geometry *Phys. Rev.* B **49** 9024
[18] Brandt E H 1996 Superconductors of finite thickness in a perpendicular magnetic field: Strips and slabs *Phys. Rev.* B **54** 4246
[19] Mataira R, Ainslie M, Badcock R and Bumby C 2020 Finite-element modelling of no-insulation HTS coils using rotated anisotropic resistivity *Supercond. Sci. Technol.* **33** 08LT01
[20] Wang X, Hahn S, Kim Y, Bascuñán J, Voccio J, Lee H and Iwasa Y 2013 Turn-to-turn contact characteristics for an equivalent circuit model of no-insulation ReBCO pancake coil *Supercond. Sci. Technol.* **26** 035012
[21] Warren W Jr and Bader W 1969 Superconductivity measurements in solders commonly used for low temperature research *Rev. Sci. Instrum.* **40** 180–2
[22] Campbell A 1982 A general treatment of losses in multifilamentary superconductors *Cryogenics* **22** 3–16